IOP Publishing Phys. Scr. 99 (2024) 105123 https://doi.org/10.1088/1402-4896/ad7911

Physica Scripta

CrossMark

OPEN ACCESS

RECEIVED
13 June 2024

REVISED
14 August 2024

ACCEPTED FOR PUBLICATION
10 September 2024

PUBLISHED
19 September 2024

PAPER

Defect-induced localization of information scrambling in 1D Kitaev model

Varadharajan Muruganandam[1,2], **Manas Sajjan**[2,3,5] **and Sabre Kais**[1,2,3,4,5,*]

[1] Department of Physics, Purdue University, West Lafayette, IN 47907, United States of America
[2] Purdue Quantum Science and Engineering Institute, Purdue University, West Lafayette, IN 47907, United States of America
[3] Department of Chemistry, Purdue University, West Lafayette, IN 47907, United States of America
[4] Elmore Family School of Electrical & Computer Engineering, Purdue University, West Lafayette, IN 47907, United States of America
[5] Department of Electrical and Computer Engineering, North Carolina State University, Raleigh, NC 27606, United States of America
[*] Author to whom any correspondence should be addressed.

E-mail: kais@purdue.edu and skais@ncsu.edu

Keywords: information scrambling, defects, Kitaev model, spin chains, out of time order correlator (OTOC)

Abstract

We discuss one-dimensional(1D) spin compass model or 1D Kitaev model in the presence of local bond defects. Three types of local disorders concerning both bond-nature and bond-strength that occur on kitaev materials have been investigated. Using exact diagonalization, two-point spin-spin structural correlations and four-point Out-of-Time-Order Correlators(OTOC) have been computed for the defective spin chains. The proposed quantities give signatures of these defects in terms of their responses to location and strength of defects. A key observation is that the information scrambling in the OTOC space gets trapped at the defect site giving rise to the phenomena of localization of information scrambling thus making these correlators a suitable diagnostic tool to detect and characterize these defects.

1. Introduction

Spin Compass Models(SCM) [1] are spin models with nearest neighbour spin-spin interactions along directions that are dependent on bond directions. A well-known SCM is the Kitaev's Honeycomb spin model which exhibits a quantum spin liquid (QSL)phase [2] supporting abelian and non-abelian anyonic excitations. This model has an exotic phase diagram with rich topological properties that offer the promise of fault-tolerant quantum computation. Along the materials side, with the recent blow-up of both theoretical and experimental studies of the iridium-oxide materials [3], the $\alpha - RuCl_3$ [4] has garnered enormous attention. Particularly, neutron scattering [5, 6] and thermal conductivity [7, 8] experiments have provided evidence that the Kitaev-type interactions dominate the physics of $\alpha - RuCl_3$ thus making them suitable candidate materials for realizing the Kitaev model. One of the main barriers in filling the gap between the theoretical predictions and real materials is the presence of defects and disorders.

Defects in real materials change the physical properties of the system that usually do not have a counterpart in their clean limit. Particularly, disorders like vacancies, impurities and lattice distortions that are inevitable in these materials contribute to instabilities [9], divergences in their density of states [10] and localization effects [11, 12]. On the other hand, such defects can also open up a plethora of new phases with unpaired majorana modes [13, 14] that arise as twist defects as proposed by Bombin [15]. These defects being the epicenter of these modes show braiding statistics that are tolerant to local perturbations. Recently, this phenomena has been generalized to arbitrary tri-valent planar lattices with Kitaev-type interactions [16]. Pertaining to these reasons, the study of defects on pristine models becomes an essential venture as a part of theoretical analysis of the aforementioned materials. Towards this direction, as a first step, we study in this article various kinds of defects on the one-dimensional(1D) analog of 2D Kitaev model i.e. 1D compass model and uncover characteristics of the system using structural and dynamical quantities. The signatures observed in these

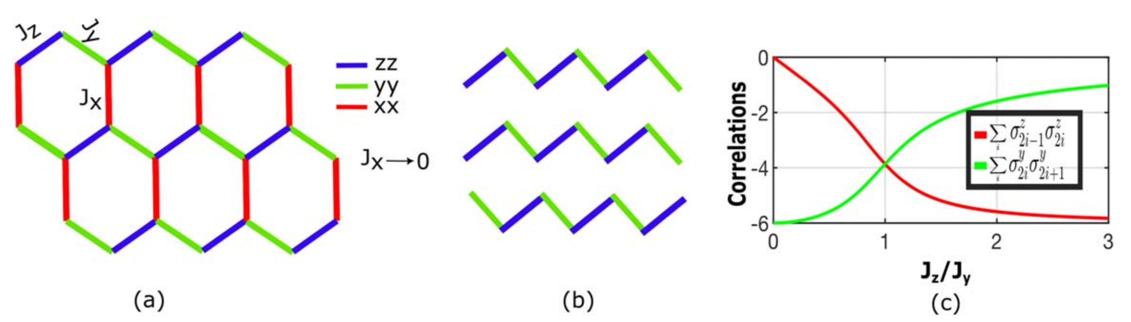

Figure 1. (a) 2D Kitaev model on a honeycomb model (b) decoupled 1D Kitaev chains (c) correlations for the clean limit of 1D Kitaev model for L = 12 spins under periodic boundary conditions(PBC).

quantities, as we shall show in the following sections serve as diagnostic tools to detect, observe and characterize the considered defects in real systems.

The paper is organized as follows: In section 2, we introduce the model, type of disorders and describe the involved metrics and numerical methods. In section 3, we present the results of disorder effects on both structural and dynamical properties of the ground state by computing different correlation measures that are introduced in the previous section. Section 4 is the conclusion.

2. Models

2.1. Kitaev models

Kitaev model in 2D is a bond-dependent interacting spin graph as shown in figure 1(a) given by the Hamiltonian,

$$H_{2\mathrm{D}} = J_x \sum_{x-bonds} \sigma_i^x \sigma_j^x + J_y \sum_{y-bonds} \times \sigma_i^y \sigma_j^y + J_z \sum_{z-bonds} \sigma_i^z \sigma_j^z \tag{1}$$

The above system belongs to the larger umbrella of SCMs wherein $(\sigma_x, \sigma_y, \sigma_z)$ denote the usual pauli matrices [17]. Such systems can also be realized on arbitrary trivalent graphs like square-octagon lattice [18–21] within cyclooctatraene based polymeric platforms [22]. Recent studies have shown that the 2D Kitaev lattice can be approximated by coupled 1D SCM chains [23–25] as shown in figure 1 and show interesting similarities [26] in terms of its phase diagram and many other physical properties. This calls us to give extra attention to the one-dimensional(1D) ZY SCM [27, 28] based on our convention. The 1D model is a bond-alternating spin-1/2 chain with bond-dependent ZZ and YY interactions as shown in 1(b). The Hamiltonian is given by,

$$H_{1\mathrm{D}} = J_z \sum_{i=1}^{N/2} \sigma_{2i-1}^z \sigma_{2i}^z + J_y \sum_{i=1}^{N/2} \sigma_{2i}^y \sigma_{2i+1}^y \tag{2}$$

where J_y, J_z are the alternating bond strengths of y-bonds and z-bonds respectively. N typically denotes the number of unit cells.

2.2. Clean limit

For the clean limit, the Kiteav model in 1D undergoes a continuous quantum phase transition(QPT) from a phase with dominating zz correlations on odd bonds for $Jz/Jy < 1$ to a phase with dominating yy correlations on even bonds for $Jz/Jy > 1$ as shown in 1(c) with transition point at $J_z = J_y$. We consider the following defects inspired by twist and on-site disorders that occur in 2D QSL model and show that in its 1D limit, the structural correlations and dynamic OTOCs can give signatures of these defects. For the sake of convenience, we have considered the ZY model and the results obtained in this article are general and remain same for XY and XZ models as well.

2.3. Defects

The pristine limit of the kitaev 1D model has alternating nature of $\sigma_z - \sigma_z$(blue) & $\sigma_y - \sigma_y$(green) bonds with alternating bond strengths Jz-Jz & Jy-Jy respectively as shown in 1(b). Any break in such alternating structure with regards to bond nature or bond strength is considered to be defective. The kind of defects that we examine in this paper are local defects that occur on a particular site concerning its local bonds. These defects are different from the usual disorders that are either taken to occur at every site or at every nearest neighbour interaction (i.e.

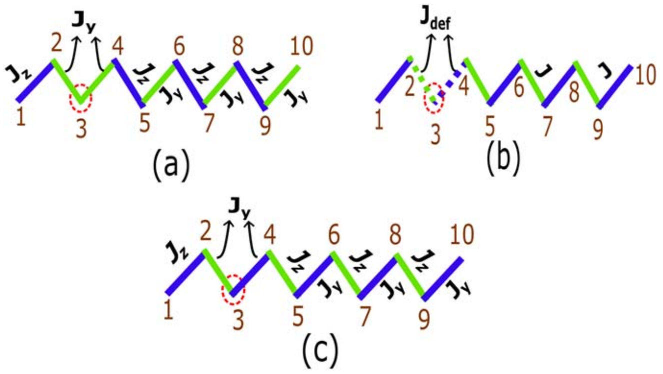

Figure 2. (a) Type 1: Bond nature-flip defect at an odd defect site 3 with yy coupling (b) Type 2: Bond-strength defect at defect site 3 with J_{def} being the bond strength of disordered bonds and J the bond strength of other bonds. (c) Type 3: Bond strength-flip defect at defect site 3 with J_y and J_z being the bond strengths as shown. (blue: $\sigma_z - \sigma_z$ bond, green: $\sigma_y - \sigma_y$ bond).

bond) that are commonly studied in spin-chains. Bond flip and bond strength defects appear both in 1D and 2D Kitaev Hamiltonians ubiquitously where the alternating structure is broken at the defect site. Firstly, we consider defect of type 1 wherein the bond nature at the vicinity of the defect site is flipped and repeated say for instance, the repeating $\sigma_y - \sigma_y$ bond at defect site 3 in figure 2(a) and the alternating nature is preserved before and after the defect. The second type concerns the bond strengths wherein the bonds at the defect have a weaker bond strength compared to the bonds elsewhere as in figure 2(b). The third type concerns the bond strength. At the vicinity of the defect site, the bond strengths are repeated while the bond natures are preserved as shown in blue and green i.e. the repeating Jy-Jy bond strengths at defect site 3 in figure 2(c). Note that in this manuscript, we do not consider the effects of defect density; rather, we focus on cases of locally single defects and explore physical quantities that can capture their signs. An additional motivation of studying these defects on a 1D model is the appearance of these defects as effective 1D line defects [29] on 2D QSL. While our analysis primarily focuses on two-point and four-point correlators for defect detection and observation, it is important to note that the introduction of these defects also modifies the energy spectrum of the spin chain, as discussed in appendix A.

3. Metrics and methods

3.1. Spin-spin correlations

We compute $\sigma_i^z \sigma_j^z$ and $\sigma_i^y \sigma_j^y$ defined as in equation (3), correlations for spin chain upto $\mathrm{L} = 12$ spins based on Exact diagonalization by employing periodic boundary conditions(PBC). Further, we compare these correlation plots with the clean limit (figure 1(c)) and look for signatures for these defects in terms of their structural correlation measures.

$$\begin{aligned} \langle \sigma_{2i-1}^z \sigma_{2i}^z \rangle &= \sum_i \langle \psi_{\mathrm{g}} | \sigma_{2i-1}^z \sigma_{2i}^z | \psi_{\mathrm{g}} \rangle \\ \langle \sigma_{2i}^y \sigma_{2i+1}^y \rangle &= \sum_i \langle \psi_{\mathrm{g}} | \sigma_{2i}^y \sigma_{2i+1}^y | \psi_{\mathrm{g}} \rangle \end{aligned} \tag{3}$$

where ψ_g denotes the ground state of the considered defective spin chain types. The index i with the sum runs over all the sites thus capturing any break in the bond nature or strength across the length of the defective spin chains.

3.2. Out-of-time-order correlator(OTOC)

Out-of-Time-Order Correlator(OTOC) first introduced by Larkin and Ovchinnikov in the context of superconductivity [30] has been exploited as a tool to provide interesting insights into physical systems. Most considerably, OTOC being a dynamic quantity quantifies how local information belonging to local degrees of freedom and operators spreads across global degrees of freedom of a quantum many-body system which is typically inaccessible to local probes. This classifies OTOC as an quantity that gives information about the scrambling dynamics of the considered physical model. Further, OTOC has found applications in the field of quantum chaos ranging from condensed matter [7, 31, 32] to high-energy physics. The key idea is the connection between the growth exponent of OTOC called the butterfly velocity of information and Lyapunov exponent indicating the onset of chaos [33–35]. Moreover, Recent proposals have shown that OTOC serves as a useful quantity to detect phase transitions such as Many-Body Localization(MBL) [36, 37]and dynamical phase transitions [32, 38, 39]. The OTOC is a 4-point correlation measure defined as

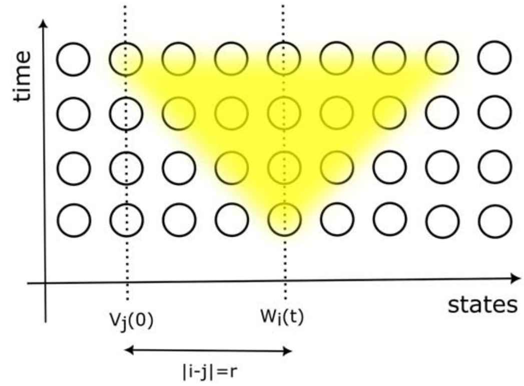

Figure 3. Space-time propagation of a general OTOC $F(r, t)$ signal.

$F_{WV}^{i,j}(t) = \langle W_i(t)V_j(0)W_i(t)V_j(0)\rangle$ where (W,V) are local operators for sites (i,j) computed at time $(t, 0)$ respectively. Further, The OTOC signal with respect to this 4-point correlation function can be defined as $F(r=|i-j|, t) = \langle W_i(t)V_j(0)W_i(t)V_j(0)\rangle$ whose space-time propagation as shown in figure 3 can give insight into information scrambling dynamics of the system thus making it a suitable probe for information propagation. OTOCs by itself is a complex quantity with the real part related to the squared commutator $C_{i,j}(t) = \langle [W_i(t), V_j(0)]^{+}[W_i(t), V_j(0)]\rangle = \langle |[W_i(t), V_j(0)]|^2\rangle = 2(1 - \mathrm{Re}[F_{i,j}(t)])$. Recently, It has been shown that the imaginary part of OTOC also possesses interesting properties of the physical system [40] that in turn is given by both commutators as well as anti-commutator of the local operators W & V respectively. The real and imaginary of the OTOC is associated to the commutator and anti-commutator as follows,

$$\langle |[W_i(t), V_j(0)]|^2\rangle = 2(1 - \mathrm{Re}[F_{WV}(r, t)]) \tag{4}$$

$$\langle [W_i(t), V_j(0)]^{+}\{W_i(t), V_j(0)\}\rangle \tag{5}$$

$$=2(1 - \mathrm{Im}[F_{WV}(r, t)]) \tag{6}$$

Since both the real and imaginary parts of OTOC in equations (4)–(6) contain the common commutator, evaluation of the commutator becomes necessary. The dynamics of OTOC is controlled by the Heisenberg evolution of $W_i(t)$ and analytical expressions for the same could be in principle derived using Baker-Campbell-Haunsdroff(BCH) expansion [41]. For our model, we choose the operator XX $(\sigma_x^i\sigma_x^j)$ as the OTOC operator based on our observations that other YY and ZZ OTOCs do not capture the information about the defects. Towards this end, we dedicate a separate section of appendix (see Appendix: C(i)) to elucidate why the YY and ZZ OTOCs do not qualify for detecting the aforementioned defects. Furthermore, if i is taken as a site residing not at the boundary, there is scattering from the open ends of the chain as illustrated in Appendix: C(ii). Therefore, we fix $i = 1$ and vary $j = 1, 2, 3......L$ in order to see how local information spreads from one end of the chain to its other end in the presence of aforementioned defects alone. The OTOC probe takes the form, $\langle\sigma_1^x(t)\sigma_j^x(0)\sigma_1^x(t)\sigma_j^x(0)\rangle$ defined as in equation (8). We compute the OTOC signal by means of Exact Diagonalization(ED) for spin chains upto L = 12 spins under open boundary conditions (OBC).

$$\langle\sigma_1^x(t)\sigma_j^x(0)\sigma_1^x(t)\sigma_j^x(0)\rangle = \tag{7}$$

$$\langle\psi_g|\sigma_1^x(t)\sigma_j^x(0)\sigma_1^x(t)\sigma_j^x(0)|\psi_g\rangle \tag{8}$$

where ψ_g denotes the ground state of the considered defective spin chain types and j is varied as $j = 1, 2, 3......L$.

4. Results

4.1. Correlation signal

In case of type 1, we plot ZZ and YY correlation functions defined by equation (3) corresponding to two different qualitative situation. i.e. when the defect is at an odd site vs when the defect is at an even site. The ordering of ZZ versus YY is symmetric as is in the clean only when the number of $\sigma_z - \sigma_z$ bonds is equal to number of $\sigma_y - \sigma_y$ bonds. We find that QPT point at $J_z = J_y$ is shifted in the case of even defect site to $J_z = 0.5\,J_y$ while it remains same for odd defect site. This is because for the former case, the total number of $\sigma_z - \sigma_z$ bonds and $\sigma_y - \sigma_y$ bonds are same and for the later case they are different. We observe that the transition point is strongly susceptible to number of bonds and is proportional to the ratio of number of $\sigma_z - \sigma_z$ bonds over the number of $\sigma_y - \sigma_y$ bonds as shown in figure 4. This relationship highlights the competition between $\sigma_z - \sigma_z$ interactions and $\sigma_y - \sigma_y$ interactions that determines the system's critical behavior. The sensitivity to bond ratio underscores

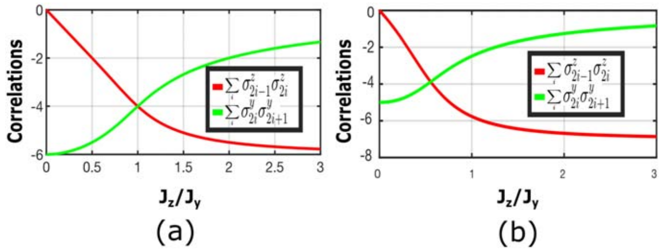

Figure 4. Type 1: (a) Correlation functions for defect at position 3 (b) Correlation functions for defect at position 6.

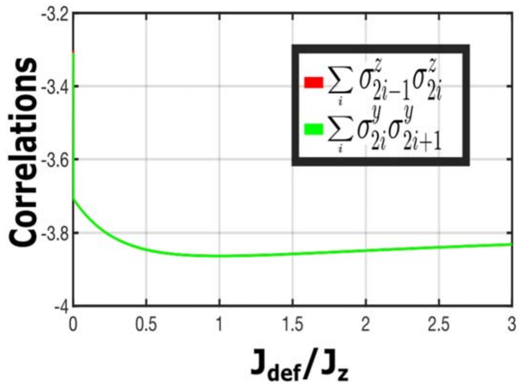

Figure 5. Type 2: Correlation functions for defect at position 4 with $J_z = J_y = 1$ and J_{def} varied w.r.t fixed J_z. Both ZZ(red) and YY(green) correlations coincide with each other.

the an-isotropic nature of the spin compass model [27], distinguishing it from isotropic systems. This proportionality suggests a scaling relationship that arises due to finite-size affects. As system size increases, we expect the transition point to converge to a fixed value in the thermodynamic limit which we leave for future analysis. However, the OTOC marker as we shall show in the following sections clearly gives distinct signatures w.r.t different considered defects.

For type 2, we fix bond strengths of the bonds that are not defective to be $J_z = J_y = J$ and vary the bond strength of the defective bonds alone with J_{def}. The ZZ and YY correlations are plotted as a function of defect strength fixing a defect site. We see that these correlations decay as we ramp the defect strength until $J_{\text{def}} = J$ post which it saturates as the entire contribution of these correlation quantities comes only from the defective bonds as shown in figure 5.

In case of type 3, we plot ZZ and YY correlation functions corresponding to two cases as taken in type 1. For the defect at site 3, The QPT at $J_z = J_y$ stays while interestingly for defect at site 6, although the ZZ and YY spin ordering follows a trend, the sharp QPT at $J_z = J_y$ is no more present. The behaviours of correlations is quite different from the case 1. For example, the ZZ correlations here are not zero when $J_z \to 0$ as only the bond strengths are disordered while the alternating bond nature exists. This contributes to finite value of the correlations as long as $J_y \neq 0$ as shown in figure 6.

4.2. OTOC signal

In this section, we plot the real and imaginary parts of the OTOC signal defined by equation (8) for 1D spin chain of length up to L = 12 for all defect types.

For type 1, the OTOC signal does not propagate beyond the defect site as evidentiated by numerical evidences in figures 7. Both the real and imaginary parts of the considered XX-OTOC entirely capture the position of the defects. These observations can further be well understood and corroborated by BCH expansion of $\sigma_1^x(t)$. In the BCH expansion of $\sigma_1^x(t)$ (See appendix B), there are annihilator-like terms (equations (B2)- B3) that prevent the growth of the operator's length beyond the defect site. Hence, the commutator which appears both in real and imaginary parts of the OTOC signal: $[\sigma_1^x(t), \sigma_j^x(0)] = 0$ for $j = d + 1, d + 2, \ldots n$ with d = defect position. This explains the observations in figures 7 wherein the information propagation as well as scrambling is absent beyond the defect site thus giving rise to the phenomenon of Localization of information scrambling.

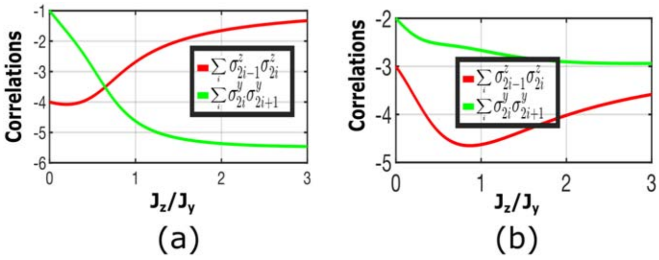

Figure 6. Type 3: (a) Correlation functions for defect at position 3 (b) Correlation functions for defect at position 6.

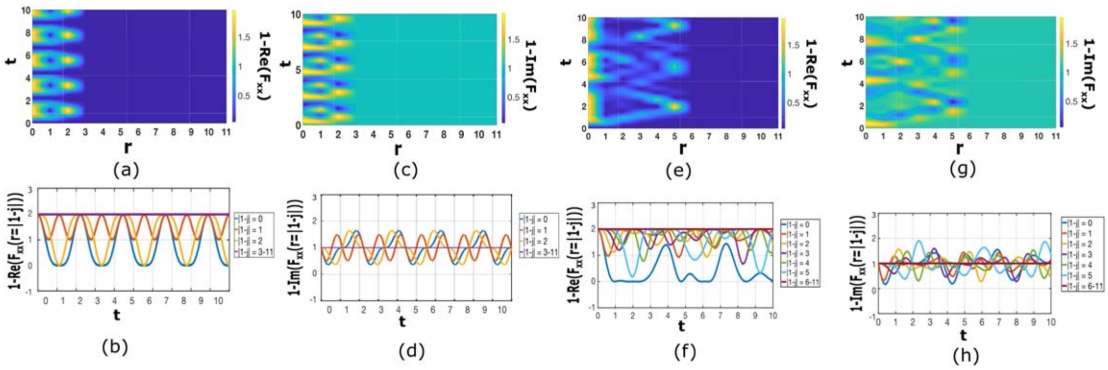

Figure 7. Type 1: (a) space-time propogation of real part of OTOC $F_{xx}(r, t)$ for defect at position 3 (b) Real part of individual OTOCs in time (c) space-time propogation of imaginary part of OTOC $F_{xx}(r, t)$ for defect at position 3 (d) imaginary part of individual OTOCs in time (e) space-time propogation of imaginary part of OTOC $F_{xx}(r, t)$ for defect at position 6 (f) Real part of individual OTOCs in time (g) space-time propogation of imaginary part of OTOC $F_{xx}(r, t)$ for defect at position 6 (h) Imaginary part of individual OTOCs in time.

The short time behavior of OTOC can be obtained by Baker-Campbell-Haunsdroff(BCH) [41] expansion and we show here closed form expressions for periodic OTOCs observed in figures 7(a) & (b) as listed in equations When the defect position is situated far from the first site, the OTOC exhibits reduced periodicity, as illustrated in figure 7(f). This loss in periodicity indicates the involvement of higher-order harmonics and the onset of scrambling, making it challenging to derive closed-form expressions using Baker-Campbell-Hausdorff (BCH) expansions. Typically, the frequency of the OTOC varies as $\sim\sqrt{J_z^2 + J_y^2}$, where J_z and J_y are the coupling strengths for the $\sigma_z - \sigma_z$ and $\sigma_y - \sigma_y$ interactions, respectively. The butterfly [42] or the scrambling time which defines the time for which local degrees of freedom scrambles into global degrees scales as $\frac{1}{\omega}$. Consequently, any alterations in bond strengths or types are reflected in the propagation patterns of these OTOCs. This relationship between the OTOC behavior and the underlying spin chain parameters provides valuable insights into the system's quantum dynamics and the impact of defects on information propagation.

$$1 - Re[\sigma_1^x(t),\, \sigma_1^x(0)\sigma_1^x(t),\, \sigma_1^x(0)] \tag{9}$$

$$= 2\sin^2(\sqrt{J_z^2 + J_y^2}\ t) \tag{10}$$

$$1 - Re[\sigma_1^x(t),\, \sigma_2^x(0)\sigma_1^x(t),\, \sigma_2^x(0)] \tag{11}$$

$$= \sin^2(2\sqrt{J_z^2 + J_y^2}\ t) \tag{12}$$

$$1 - Re[\sigma_1^x(t),\, \sigma_3^x(0)\sigma_1^x(t),\, \sigma_3^x(0)] \tag{13}$$

$$= \sin^2(\sqrt{J_z^2 + J_y^2}\ t) \tag{14}$$

For type 2, the OTOC signal propagates giving signs of the defect as the bond strength of the defective bonds J_{def} is increased as in figure 8. Both the real and imaginary parts of the considered XX-OTOC captures the defects (marked in red). The reason for these observations is understood by the BCH expansion of $\sigma_1^x(t)$. In the BCH expansion of $\sigma_1^x(t)$, the annihilator-like terms as in B4 for type 2 defects, has an amplitude or weight that depends on the defective bond strength J_{def}. This explains the observations in figures 8 wherein the information propagation as well as scrambling is localized in the illustrated fashion giving necessary signs of the defects.

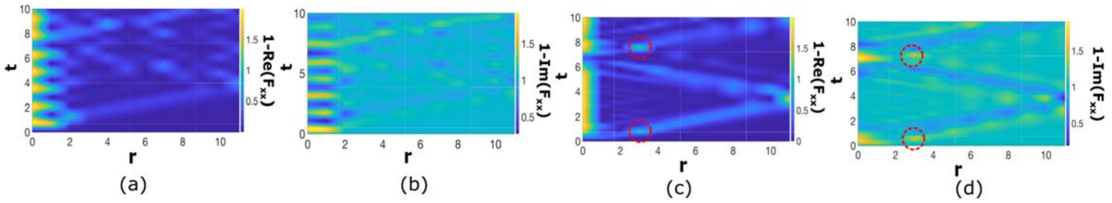

Figure 8. Type 2, for $J_z = J_y = 1$, (a) space-time propagation of real part of OTOC $F_{xx}(r, t)$ for defect at position 3 for $J_{\mathrm{def}} = 0.5$ (defective bond strength) (b) space-time propagation of imaginary part of OTOC $F_{xx}(r, t)$ for defect at position 3 for $J_{\mathrm{def}} = 0.5$ (defective bond strength) (c) space-time propagation of real part of OTOC $F_{xx}(r, t)$ for defect at position 3 for $J_{\mathrm{def}} = 2$ (OTOC sign at the defect site marked in red) (d) space-time propagation of imaginary part of OTOC $F_{xx}(r, t)$ for defect at position 3 for $J_{\mathrm{def}} = 2$ (OTOC sign at the defect site marked in red).

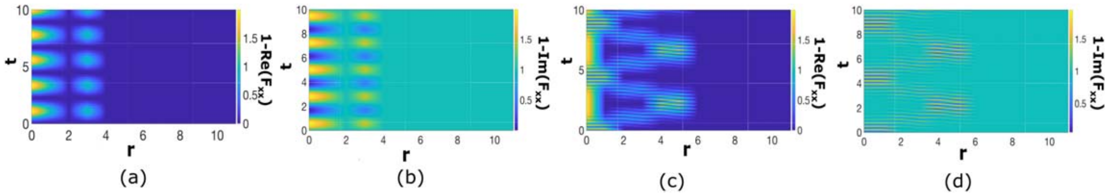

Figure 9. Type 3, (a) space-time propagation of real part of OTOC $F_{xx}(r, t)$ for defect at position 3 with $J_y = 10, Jz = .1$ (b) space-time propagation of imaginary part of OTOC $F_{xx}(r, t)$ for defect at position 3 with $J_y = 10, Jz = .1$ (c) space-time propagation of real part of OTOC $F_{xx}(r, t)$ for defect at position 6 with $J_y = .1, Jz = 1$ (d) space-time propagation of imaginary part of OTOC $F_{xx}(r, t)$ for defect at position 6 with $J_y = .1, Jz = 1$ (site 3 corresponds to odd site so $J_y > J_z$ and site 6 corresponds to even site i.e. $J_z > J_y$ as elucidated above).

For type 3, the OTOC signal does not propagate beyond the defect site as shown in figure 9. Similar to the above cases, both the real and imaginary parts of the considered XX-OTOC capture defect signatures. The annihilator-like terms (equations (B5)- B6) in the BCH expansion of $\sigma_1^x(t)$ has an amplitude that depends on the ratio $\frac{1}{J_y}$ for an odd defect site and ratio $\frac{1}{J_z}$ for even defect site. By tuning this ratio, OTOC signal can be made localized thus giving suitable signs of the defects.

5. Conclusion

We have studied defects on pristine 1D Kitaev model using structural and dynamical quantities. We have presented ways to realize three types of disorders that are prevalent in Kitaev materials. In particular, the effects of disorder on the spin-spin correlations and OTOCs within the ground-state manifold of our defective models have been investigated. We have considered 3 types of disorder: bond nature-flip, bond-strength, bond strength-flip disorders. Though these disorders are quite different, they behave similar in terms of their responses to the OTOC signal probe i.e. they cause localization in the OTOC space thus illustrating prohibited information scrambling across the length of the spin-chain. Regardless of this localization phenomena, the disorders show quite unique signatures of themselves in the OTOC space. This makes OTOCs as suitable detection tools susceptible to different defects in the model. In terms of physical realization, not only can OTOCs be measured in an experimental setup [43], circuit-based measurements of OTOCs on state-of the art quantum computers have also been achieved [44–47]. Moreover, in superconducting Circuit quantum electrodynamics(CQED) setting [48], the above-discussed defective models can be realized using superconducting circuits [45, 49] wherein the defective qubit along with its local bonds can be used as a control qubit that controls the entire scrambling dynamics of the circuit.

Though we have considered only time-independent and static disorders, the OTOC signal proposed in this article, given its spatio-temporal dependence can be used to detect time-dependent perturbations too upon the clean model. A special consideration is floquet or periodic time-dependent perturbations wherein the relevant quantity to consider is the Floquet OTOC [39, 50, 51]. Such systems have shown to exhibit interesting phases such as time crystals and MBL [52–55]. These reasons serve as motivating factors for a future study of these phases in 1D kitaev model. Additionally, as a natural extension, study of OTOC propagation in 2D Kitaev model can give insights into defects and fundamental excitations. Apart from exploring higher dimensions, another promising future direction is to extend our analysis to larger system sizes using advanced numerical techniques such as tensor network methods [56, 57]. In this manuscript, the stability of the results has been checked for spin

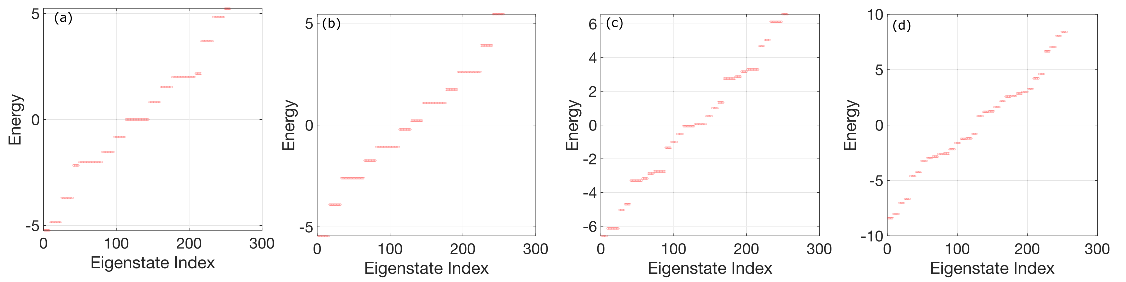

Figure 10. (a) Eigenenergy spectrum for L = 8 spins of the clean model as defined in equation (2) for $J_z = J_y = 1$ (b) Eigenenergy spectrum for L = 8 spins for defect type 1 at position 3 with $J_z = J_y = 1$ (c) Eigenenergy spectrum for L = 8 spins for defect type 2 with for $J_z = J_y = 1$ and $J_{def} = 2$ at position 3 (d) Eigenenergy spectrum for L = 8 spins for defect type 2 with for $J_z = 1, J_y = 2$ at position 3 (Note: All analysis is done with periodic chains-PBC).

chains of length ranging from 8 to 14 spins using ED(see appendix D). Advanced techniques will allow us to investigate the behavior of bulk spins and their contribution to information scrambling in the presence of defects, and insights into bulk-boundary correspondence [58]. Such investigations will provide valuable insights into the interplay between local defects and global properties of the system, including topological order and long-range entanglement [59, 60].

Acknowledgments

The authors would like to acknowledge the financial support from the Quantum Science Center, a National Quantum Information Science Research Center of the U.S. Department of Energy (DOE).

Data availability statement

All data that support the findings of this study are included within the article (and any supplementary files).

Conflict of interest

The authors declare no conflicts of interest.

Ethics statement

The authors confirm that they have followed the ethical policies of the journal.

Appendix A. Eigenenergy spectrum

In this section, we present the eigen-energy spectrum for both the clean model and various defective cases. The eigen-energy spectrum for the clean model is depicted in figure 10(a). This serves as the baseline for comparison with defective cases, where the system's inherent symmetries result in certain degeneracies within the energy bands.

For defect-type 1, the introduction of an additional ZZ interaction at defect site 3 leads to the splitting of energy bands, as illustrated in figure 10(b). This band splitting signifies the lifting of degeneracies present in the original model, a direct consequence of the symmetry breaking induced by the defect. In the case of defect-type 2, which involves a bond strength defect, the defective bond causes not only a splitting of the energy bands but also a modification of the overall energy scale of the system. The extent of these changes is dependent on the strength of the defective bond. Similarly, defect-type 3, characterized by a bond strength flip defect, results in the splitting of energy bands and an alteration of the systems energy scale. These effects are influenced by the bond strengths J_y & J_z as depicted in figure 10(d). In summary, the introduction of defects into the system leads to both the breaking of degeneracies and changes in the scale of eigenenergies. These alterations are dependent on the nature and strength of the defects introduced.

Appendix B. Time evolution of $\sigma_1^x(t)$

The time evolution of $\sigma_1^x(t)$ is given by Heisenberg time evolution which can be further expanded with the help of Baker-Campbell-Haunsdroff(BCH) [41] formula as,

$$\begin{aligned}\sigma_1^x(t) &= e^{iHt}\sigma_1^x(0)e^{-iHt}\\ &= \sigma_1^x(0) + it\left[H, \sigma_1^x] + \frac{(it)^2}{2!}[H, [H, \sigma_1^x]] + \ldots\ldots \frac{(it)^n}{n!}[H, \sigma_1^x\right]_n\end{aligned} \tag{B1}$$

where $[H, \sigma_1^x(t)]_n$ is the nested commutator obtained after computing $[H, [H, \ldots \text{n times} \ldots [H, \sigma_1^x(t)]$.

B.1. Type 1

- ***case 1***: When defect occurs at an odd site, the defective bond is a y-y bond, thus resulting in the hamiltonian,

$$\begin{aligned}H = J(&\sigma_1^z\sigma_2^z + \sigma_2^y\sigma_3^y + \sigma_3^z\sigma_4^z + \ldots\ldots\ldots\ldots + \sigma_{d-2}^z\sigma_{d-1}^z\\ &+ \underbrace{\sigma_{d-1}^y\sigma_d^y + \sigma_d^y\sigma_{d+1}^y}_{\text{defective bond}} + \sigma_{d+1}^z\sigma_{d+2}^z + \sigma_{d+2}^y\sigma_{d+3}^y + \ldots\ldots\ldots\ldots\end{aligned}$$

where d=defect position. $\sigma_1^x(t)$ under the evolution of the above Hamiltonian has the form,

$$\sigma_1^x(t) = \sigma_1^x(0) + it(J2i\sigma_1^y\sigma_2^z)\ldots\ldots\ldots \underbrace{+\frac{(it)^{d-1}}{(d-1)!}2^{d-1}i^{d-1}J^{d-1}\sigma_1^y\sigma_1^x\ldots\ldots\sigma_{d-1}^x\sigma_d^y}_{\text{Annihilator}} \tag{B2}$$

- ***case 2***: When defect occurs at an even site, the defective bond is a z-z bond, thus resulting in the Hamiltonian,

$$\begin{aligned}H = J(&\sigma_1^z\sigma_2^z + \sigma_2^y\sigma_3^y + \sigma_3^z\sigma_4^z + \ldots\ldots\ldots\ldots + \sigma_{d-2}^y\sigma_{d-1}^y\\ &+ \underbrace{\sigma_{d-1}^z\sigma_d^z + \sigma_d^z\sigma_{d+1}^z}_{\text{defective bond}} + \sigma_{d+1}^y\sigma_{d+2}^y + \sigma_{d+2}^z\sigma_{d+3}^z + \ldots\ldots\ldots\ldots\end{aligned}$$

where d=defect position. $\sigma_1^x(t)$ under the evolution of the above Hamiltonian has the form,

$$\sigma_1^x(t) = \sigma_1^x(0) + it(J2i\sigma_1^y\sigma_2^z)\ldots\ldots\ldots \underbrace{+\frac{(it)^{d-1}}{(d-1)!}2^{d-1}i^{d-1}J^{d-1}\sigma_1^y\sigma_1^x\ldots\ldots\sigma_{d-1}^x\sigma_d^z}_{\text{Annihilator}} \tag{B3}$$

The operator of the annihilator terms in the BCH expansion gets terminated with $\sigma_d^z(\sigma_d^y)$ for odd d(even d) correspondingly that prohibits their growth. This in turn, results in the commutator:
$[\sigma_1^x(t), \sigma_j^x(0)] = 0$ for $j \geqslant d + 1$ with $d =$ defect position.

B.2. Type 2

When defect occurs at a site d, it results in the Hamiltonian,

$$\begin{aligned}H = J(&\sigma_1^z\sigma_2^z + \sigma_2^y\sigma_3^y + \sigma_3^z\sigma_4^z + \ldots\ldots\ldots\ldots + \sigma_{d-2}^z\sigma_{d-1}^z)\\ &+ J_{\text{def}}(\underbrace{\sigma_{d-1}^y\sigma_d^y + \sigma_d^z\sigma_{d+1}^z}_{\text{defect}}) + J(\sigma_{d+1}^z\sigma_{d+2}^z + \sigma_{d+2}^y\sigma_{d+3}^y + \ldots\ldots\ldots\ldots\end{aligned}$$

where d=defect position. $\sigma_1^x(t)$ under the evolution of the above Hamiltonian has the form,

$$\sigma_1^x(t) = \sigma_1^x(0) + it(J2i\sigma_1^y\sigma_2^z)\ldots\ldots\ldots \underbrace{+\frac{(it)^{d-1}}{(d-1)!}2^{d-1}i^{d-1}\frac{J^d}{J_{\text{def}}}\sigma_1^y\sigma_1^x\ldots\ldots\sigma_{d-1}^x\sigma_d^x}_{\text{Annihilator}} + \ldots\ldots\ldots \tag{B4}$$

As the bond strength J_{def} is gradually ramped up, the weight of the operator $\sigma_1^y\sigma_1^x\ldots\ldots\sigma_{d-1}^x\sigma_d^x$ dies down due to which the subsequent nested commutators in the BCH expansion is heavily attenuated giving rise to OTOC localization as illustrated in the main text of this article.

B.3. Type 3

- ***case 1***: When defect occurs at an odd site, it results in the hamiltonian,

$$H = J_z\sigma_1^z\sigma_2^z + J_y\sigma_2^y\sigma_3^y + \sigma_3^z\sigma_4^z + \ldots\ldots\ldots\ldots + \sigma_{d-2}^z\sigma_{d-1}^z$$
$$+ \underbrace{J_y\sigma_{d-1}^y\sigma_d^y + J_y\sigma_d^z\sigma_{d+1}^z}_{\text{defect}} + J_z\sigma_{d+1}^y\sigma_{d+2}^y + J_y\sigma_{d+2}^z\sigma_{d+3}^z + \ldots\ldots\ldots\ldots$$

where d=defect position. $\sigma_1^x(t)$ under the evolution of the above Hamiltonian has the form,

$$\sigma_1^x(t) = \sigma_1^x(0) + it(J_z 2i\sigma_1^y\sigma_2^z)\ldots\ldots\ldots + \underbrace{\frac{(it)^{d-1}}{(d-1)!}2^{d-1}i^{d-1}\frac{(J_zJ_y)^d}{J_y}\sigma_1^y\sigma_1^x\ldots\ldots\sigma_{d-1}^x\sigma_d^y}_{\text{Annihilator}} \tag{B5}$$

- ***case 2***: When defect occurs at an even site, it results in the hamiltonian,

$$H = J_z\sigma_1^z\sigma_2^z + J_y\sigma_2^y\sigma_3^y + \sigma_3^z\sigma_4^z + \ldots\ldots\ldots\ldots + \sigma_{d-2}^y\sigma_{d-1}^y$$
$$+ \underbrace{J_z\sigma_{d-1}^z\sigma_d^z + J_z\sigma_d^y\sigma_{d+1}^y}_{\text{defect}} + J_y\sigma_{d+1}^z\sigma_{d+2}^z + J_z\sigma_{d+2}^y\sigma_{d+3}^y + \ldots\ldots\ldots\ldots$$

where d=defect position. $\sigma_1^x(t)$ under the evolution of the above Hamiltonian has the form,

$$\sigma_1^x(t) = \sigma_1^x(0) + it(J_z 2i\sigma_1^y\sigma_2^z)\ldots\ldots\ldots + \underbrace{\frac{(it)^{d-1}}{(d-1)!}2^{d-1}i^{d-1}\frac{(J_zJ_y)^d}{J_z}\sigma_1^y\sigma_1^x\ldots\ldots\sigma_{d-1}^x\sigma_d^z}_{\text{Annihilator}} \tag{B6}$$

Appendix C. Analysis of other OTOC probes

In this appendix, we present a detailed analysis of the behavior of YY/ZZ and other OTOC probes in the presence of defects, and discuss their limitations in distinguishing between different defect configurations.

(i) **YY & ZZ OTOCS:** The YY OTOC probe, $\langle\sigma_1^y(t)\sigma_j^y(0)\sigma_1^y(t)\sigma_j^y(0)\rangle$ fails to distinguish between defects at odd and even sites. For example, at defect position d = 2 for type 1, the evolution is given by:

$$\sigma_1^y(t,\, d=2) = \sigma_1^y(0) + it(-2iJ\sigma_1^x\sigma_2^z) + \frac{(it)^2}{2!}(-4J^2\sigma_1^y) + \frac{(it)^3}{3!}(-8iJ^3\sigma_1^x\sigma_2^z) + \ldots\ldots \tag{C1}$$

While at position d = 3,

$$\sigma_1^y(t,\, d=3) = \sigma_1^y(0) + it(-2iJ\sigma_1^x\sigma_2^z) + \frac{(it)^2}{2!}4J^2(\sigma_1^y + \sigma_1^x\sigma_2^x\sigma_3^y) \tag{C2}$$

$$+\frac{(it)^3}{3!}8iJ^3(-2\sigma_1^x\sigma_2^z + \sigma_1^y\sigma_2^x\sigma_3^y + \sigma_1^z\sigma_1^x\sigma_2^y\sigma_3^y) + \ldots\ldots \tag{C3}$$

This leads us to $[\sigma_1^y(t,\, d=2),\, \sigma_j^y(0)] = [\sigma_1^y(t,\, d=3),\, \sigma_j^y(0)] = 0$ for $j = 3, 4,\ldots L$ indicating no distinction between odd and even defect sites.

On the other hand, the ZZ OTOC $\langle\sigma_1^z(t)\sigma_j^z(0)\sigma_1^z(t)\sigma_j^z(0)\rangle$ shows no evolution at all. For instance:

$$\sigma_1^z(t,\, d=2) = \sigma_1^z(0) \text{ and } \sigma_1^z(t,\, d=3) = \sigma_1^z(0) \tag{C4}$$

As a result, defects are not captured by the chosen ZZ and YY OTOCs, rendering them unsuitable for detecting the defects considered in this study.

(ii) **XX-OTOC with $i \neq 0, L$:** If the OTOC probe is defined as $\langle\sigma_i^x(t)\sigma_j^x(0)\sigma_i^x(t)\sigma_j^x(0)\rangle$ for $i \neq 1, L$ i.e. that is, when the initial site i is not at the boundarywe observe a qualitative difference. Specifically, the OTOC scatters from the end of the chain where the defect is absent. On the other hand, when examining the side of the chain where the defect is present, the OTOC propagation exhibits localization behavior as illustrated in figure 11.

Appendix D. Longer chains

To verify stability across system sizes, we analyzed OTOC propagation in spin chains from 8 to 14 spins using numerical exact diagonalization as illustrated in figure 12. Our findings show that defect-induced localization of information scrambling is consistent across all system sizes, confirming the effectiveness of OTOCs for defect detection. This supports our results and sets the stage for future studies on larger systems.

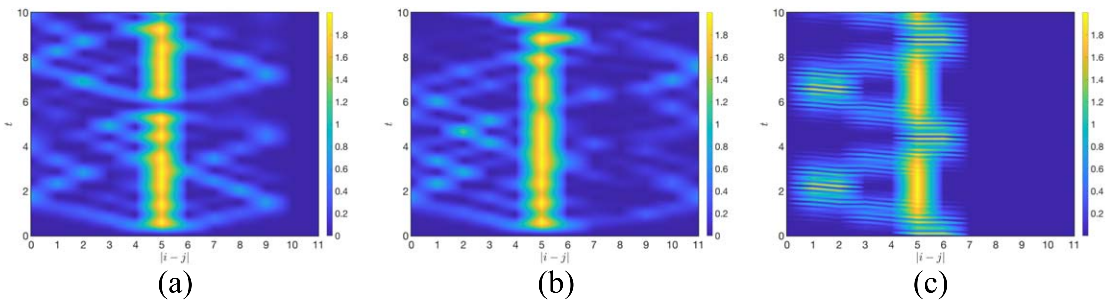

Figure 11. OTOC ($1 - \mathrm{Re}[\langle \sigma_4^x(t)\sigma_j^x(0)\sigma_4^x(t)\sigma_j^x(0)\rangle]$) propagation: (a) In the presence of defect 1 at position 9. (b) In the presence of defect 2 at position 9. (c) In the presence of defect 3 at position 9.

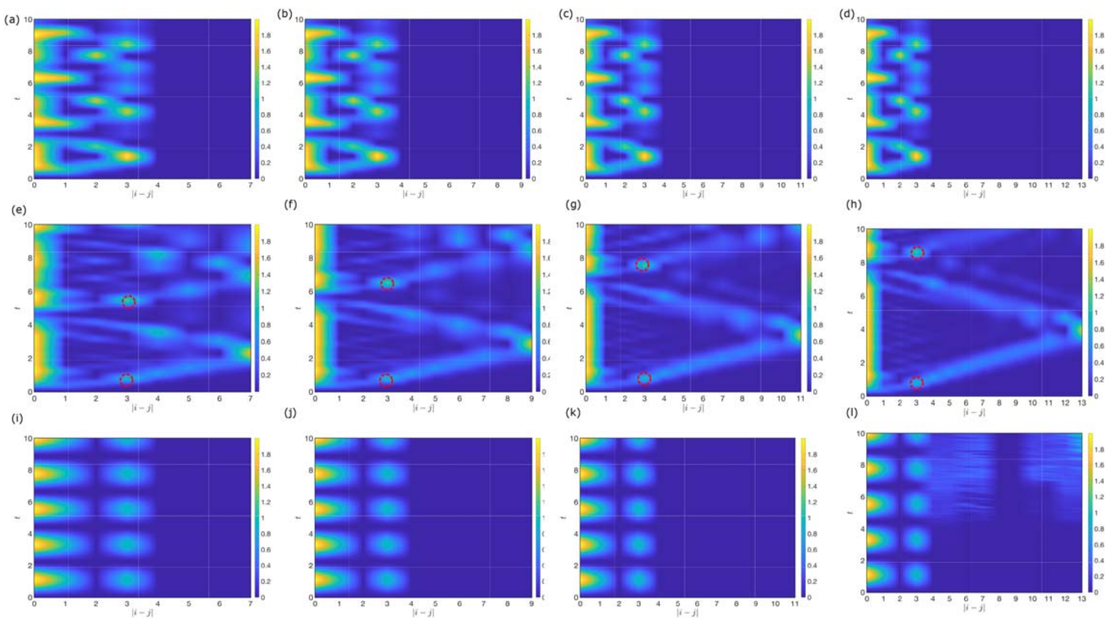

Figure 12. OTOC ($1 - \mathrm{Re}[\langle \sigma_1^x(t)\sigma_j^x(0)\sigma_1^x(t)\sigma_j^x(0)\rangle]$) propagation: (a)-(d) In the presence of defect 1 at position 3 for spin chains of lengths L = 8, 10, 12, 14 respectively. (e)-(h) In the presence of defect 2 at position 3 for spin chains of lengths L = 8, 10, 12, 14 respectively. (i)-(l) In the presence of defect 3 at position 3 for spin chains of lengths L = 8, 10, 12, 14 respectively.

ORCID iDs

Varadharajan Muruganandam https://orcid.org/0000-0001-7888-2603
Manas Sajjan https://orcid.org/0000-0001-7436-5422
Sabre Kais https://orcid.org/0000-0003-0574-5346

References

[1] Nussinov Z and Brink J v d 2015 Compass models: Theory and physical motivations *Rev. Mod. Phys.* **87** 1–59
[2] Kitaev A 2006 Anyons in an exactly solved model and beyond *Ann. Phys.* **321** 2–111
[3] Jackeli G and Khaliullin G 2009 Mott insulators in the strong spin-orbit coupling limit: From heisenberg to a quantum compass and kitaev models *Phys. Rev. Lett.* **102** 017205
[4] Koitzsch A, Habenicht C, Müller E, Knupfer M, Büchner B, Kandpal H C, Van Den Brink J, Nowak D, Isaeva A and Doert T 2016 J eff description of the honeycomb mott insulator α- rucl 3 *Phys. Rev. Lett.* **117** 126403
[5] Banerjee A *et al* 2016 Proximate kitaev quantum spin liquid behaviour in a honeycomb magnet *Nat. Mater.* **15** 733–40
[6] Banerjee A, Yan J, Knolle J, Bridges C A, Stone M B, Lumsden M D, Mandrus D G, Tennant D A, Moessner R and Stephen S E 2017 Neutron scattering in the proximate quantum spin liquid α-rucl3 *Science* **356** 1055–9
[7] Patel A A, Chowdhury D, Sachdev S and Swingle B 2017 Quantum butterfly effect in weakly interacting diffusive metals *Phys. Rev.* X **7** 031047
[8] Hirobe D, Sato M, Shiomi Y, Tanaka H and Saitoh E 2017 Magnetic thermal conductivity far above the néel temperature in the kitaev-magnet candidate $\alpha - \mathrm{rucl}_3$ *Phys. Rev.* B **95** 241112

[9] Andrade E C, Janssen L and Vojta M 2020 Susceptibility anisotropy and its disorder evolution in models for kitaev materials *Physical Review B* **102** 115160

[10] Knolle J, Moessner R and Perkins N B 2019 Bond-disordered spin liquid and the honeycomb iridate $h_3liir_2o_6$: abundant low-energy density of states from random majorana hopping *Phys. Rev. Lett.* **122** 047202

[11] Willans A J, Chalker J T and Moessner R 2010 Disorder in a quantum spin liquid: flux binding and local moment formation *Phys. Rev. Lett.* **104** 237203

[12] Kao W-H and Perkins N B 2021 Disorder upon disorder: localization effects in the kitaev spin liquid *Ann. Phys.* **435** 168506

[13] Petrova O, Mellado P and Tchernyshyov O 2013 Unpaired majorana modes in the gapped phase of kitaev's honeycomb model *Phys. Rev.* B **88** 140405

[14] Petrova O, Mellado P and Tchernyshyov O 2014 Unpaired majorana modes on dislocations and string defects in kitaev's honeycomb model *Phys. Rev.* B **90** 134404

[15] Bombin H 2010 Topological order with a twist: Ising anyons from an abelian model *Phys. Rev. Lett.* **105** 030403

[16] Yan B and Cui S X 2023 Generalized kitaev spin liquid model and emergent twist defect arXiv:2308.06835

[17] Sakurai J J and Napolitano J 2020 *Modern Quantum Mechanics* (Cambridge University Press)

[18] Yang S, Zhou D L and Sun C P 2007 Mosaic spin models with topological order *Phys. Rev.* B **76** 180404

[19] Kells G, Kailasvuori J, Slingerland J K and Vala J 2011 Kaleidoscope of topological phases with multiple majorana species *New J. Phys.* **13** 095014

[20] Yamada M G, Dwivedi V and Hermanns M 2017 Crystalline kitaev spin liquids *Phys. Rev.* B **96** 155107

[21] Yamada M G 2021 Topological Z_2 invariant in kitaev spin liquids: classification of gapped spin liquids beyond projective symmetry group *Phys. Rev. Res.* **3** L012001

[22] Muruganandam V, Sajjan M and Kais S 2023 Foray into the topology of poly-bi-[8]-annulenylene *Natural Sciences* **3** e20230015

[23] Agrapidis C E, Brink J v d and Nishimoto S 2018 Ordered states in the kitaev-heisenberg model: From 1d chains to 2d honeycomb *Sci. Rep.* **8** 1815

[24] Agrapidis C E, Brink J v d and Nishimoto S 2019 Ground state and low-energy excitations of the kitaev-heisenberg two-leg ladder *Phys. Rev.* B **99** 224418

[25] Feng S, Agarwala A and Trivedi N 2024 *Dimensional Reduction of Kitaev Spin Liquid at Quantum Criticality* **6** 013298

[26] Feng S, Agarwala A, Bhattacharjee S and Trivedi N 2023b Anyon dynamics in field-driven phases of the anisotropic kitaev model *Phys. Rev.* B **108** 035149

[27] Brzezicki W, Dziarmaga J and Oleś A M 2007 Quantum phase transition in the one-dimensional compass model *Physical Review B* **75** 134415

[28] Eriksson E and Johannesson H 2009 Multicriticality and entanglement in the one-dimensional quantum compass model *Phys. Rev.* B **79** 224424

[29] Freitas L R D and Pereira R G 2022 Gapless excitations in non-abelian kitaev spin liquids with line defects *Phys. Rev.* B **105** L041104

[30] Larkin A I and Ovchinnikov Y N 1969 Quasiclassical method in the theory of superconductivity *Sov. Phys. JETP* **28** 1200–5

[31] Dóra B and Moessner R 2017 Out-of-time-ordered density correlators in luttinger liquids *Phys. Rev. Lett.* **119** 026802

[32] Heyl M, Pollmann F and Dóra B 2018 Detecting equilibrium and dynamical quantum phase transitions in ising chains via out-of-time-ordered correlators *Phys. Rev. Lett.* **121** 016801

[33] Maldacena J, Shenker S H and Stanford D 2016 A bound on chaos *J. High Energy Phys.* **2016**

[34] Shenker S H and Stanford D 2014 Black holes and the butterfly effect *J. High Energy Phys.* **2014** 1–25

[35] Gu Y, Qi X-L and Stanford D 2017 Local criticality, diffusion and chaos in generalized sachdev-ye-kitaev models *J. High Energy Phys.* **2017** 1–37

[36] Riddell J and Sørensen E S 2019 Out-of-time ordered correlators and entanglement growth in the random-field xx spin chain *Phys. Rev.* B **99** 054205

[37] Lee J, Kim D and Kim D-H 2019 Typical growth behavior of the out-of-time-ordered commutator in many-body localized systems *Phys. Rev.* B **99** 184202

[38] Nie X *et al* 2020 Experimental observation of equilibrium and dynamical quantum phase transitions via out-of-time-ordered correlators *Phys. Rev. Lett.* **124** 250601

[39] Zamani S, Jafari R and Langari A 2022 Out-of-time-order correlations and floquet dynamical quantum phase transition *Phys. Rev.* B **105** 094304

[40] Sajjan M, Singh V, Selvarajan R and Kais S 2023 Imaginary components of out-of-time-order correlator and information scrambling for navigating the learning landscape of a quantum machine learning model *Physical Review Research* **5** 013146

[41] Hall B C and Hall B C 2013 *Lie Groups, Lie Algebras, and Representations* (Springer)

[42] Cotler J S, Ding D and Penington G R 2018 Out-of-time-order operators and the butterfly effect *Ann. Phys.* **396** 318–33

[43] Martin Gärttner J G, Bohnet A, Safavi-Naini M L, Wall J J and Rey A M 2017 Measuring out-of-time-order correlations and multiple quantum spectra in a trapped-ion quantum magnet *Nat. Phys.* **13** 781–6

[44] Zhu Q *et al* 2022 Observation of thermalization and information scrambling in a superconducting quantum processor *Phys. Rev. Lett.* **128** 160502

[45] Blok M S, Ramasesh V V, Schuster T, O'Brien K, Kreikebaum J M, Dahlen D, Morvan A, Yoshida B, Yao N Y and Siddiqi I 2021 Quantum information scrambling on a superconducting qutrit processor *Phys. Rev.* X **11** 021010

[46] Landsman K A, Figgatt C, Schuster T, Linke N M, Yoshida B, Yao N Y and Monroe C 2019 Verified quantum information scrambling *Nature* **567** 61–5

[47] Joseph Harris B Y and Nikolai A S 2022 Benchmarking information scrambling *Phys. Rev. Lett.* **129** 050602

[48] Blais A, Huang R-S, Wallraff A, Girvin S M and Schoelkopf R J 2004 Cavity quantum electrodynamics for superconducting electrical circuits: An architecture for quantum computation *Phys. Rev.* A **69** 062320

[49] Chávez-Carlos J, Lezama T L M, Cortiñas R G, Venkatraman J, Devoret M H, Batista V S, Pérez-Bernal F and Santos L F 2023 Spectral kissing and its dynamical consequences in the squeeze-driven kerr oscillator *npj. Quantum Information* **9** 76

[50] Jafari R, Akbari A, Mishra U and Johannesson H 2022 Floquet dynamical quantum phase transitions under synchronized periodic driving *Phys. Rev.* B **105** 094311

[51] Shukla R K and Mishra S K 2022 Characteristic, dynamic, and near-saturation regions of out-of-time-order correlation in floquet ising models *Phys. Rev.* A **106** 022403

[52] Else D V, Bauer B and Nayak C 2016 Floquet time crystals *Phys. Rev. Lett.* **117** 090402

[53] Huang B, Wu Y-H and Liu W V 2018 Clean floquet time crystals: models and realizations in cold atoms *Phys. Rev. Lett.* **120** 110603

[54] Khemani V, Moessner R and Sondhi S L 2019 *A Brief History of Time Crystals* arXiv:1910.10745

[55] Zaletel M P, Lukin M, Monroe C, Nayak C, Wilczek F and Norman N Y 2023 Colloquium: quantum and classical discrete time crystals *Rev. Mod. Phys.* **95** 031001
[56] Schollwöck U 2011 The density-matrix renormalization group in the age of matrix product states *Ann. Phys.* **326** 96–192
[57] Biamonte J and Bergholm V 2017 Tensor networks in a nutshell arXiv:1708.00006
[58] Estarellas M P, D'Amico I and Spiller T P 2017 Topologically protected localised states in spin chains *Sci. Rep.* **7** 42904
[59] Fagotti M 2016 Charges and currents in quantum spin chains: late-time dynamics and spontaneous currents *J. Phys. A: Math. Theor.* **50** 034005
[60] Apollaro T J G and Plastina F 2006 Entanglement localization by a single defect in a spin chain *Physical Review Atomic, Molecular, and Optical Physics* **74** 062316